Environmental Science and Pollution Research (2023) 30:28818–28829
https://doi.org/10.1007/s11356-022-24225-9

RESEARCH ARTICLE

Alpinia officinarum mediated copper oxide nanoparticles: synthesis and its antifungal activity against *Colletotrichum gloeosporioides*

Chunmei Hu[1] · Wenjia Zhu[1] · Ying Lu[1] · Yanfang Ren[1,2] · Jinyu Gu[1] · Yaping Song[1] · Junyu He[1,2]

Received: 7 April 2022 / Accepted: 11 November 2022 / Published online: 19 November 2022

Abstract

Green synthesis offers an environmentally friendly and cost-effective alternative for the synthesis of copper oxide nanoparticles (CuO NPs). In this study, the synthesis of CuO NPs was optimized by using copper sulfate ($CuSO_4$) and the aqueous extract of *Alpinia officinarum* and its antifungal activity were investigated. The synthesized CuO NPs were characterized by UV–visible spectroscopy (UV–vis), X-ray diffraction (XRD), Fourier-transform infrared radiation spectroscopy (FT-IR), scanning electron microscope (SEM), energy dispersive spectroscopy (EDS), dynamic light scattering (DLS), and transmission electron microscopy (TEM). The results showed that the optimized conditions for the synthesis of CuO NPs were 1:2 ratio of extract and $CuSO_4$ solution, pH 7, and 30 °C. The characteristic UV–vis peak of *A. officinarum* synthesized CuO NPs was at 264 nm. The synthesized CuO NPs had high crystallinity and purity and were spherical in morphology with the mean size of 46.40 nm. The synthesized CuO NPs reduced the fungal growth of *Colletotrichum gloeosporioides* in a dose-dependent manner. The minimum inhibitory concentration (MIC) and minimum fungicidal concentration (MFC) of the CuO NPs were 125 μg·mL^{-1} and 500 μg·mL^{-1}, respectively. The antifungal activity of CuO NPs may be attributed to its ability to deform the structure of fungal hyphae, induce excessive reactive oxygen species accumulation and lipid peroxidation in fungi, disrupt the mycelium cell membrane, and result cellular leakage.

Keywords Green synthesis · CuO NPs · *Alpinia officinarum* · *Colletotrichum gloeosporioides* · Antifungal activity

Introduction

In recent years, nanotechnology has been emerging as an advanced technology and widely used in the fields of industry, agriculture, medicine, etc. (Murugesan et al. 2019). Nanoparticles (NPs) exhibit unique physicochemical properties compared with their bulk materials, such as huge specific surface area, high activity, and good optical and electrical conductivity (Moon et al. 2018). Copper oxide (CuO), as an important transition metal oxide, has attracted wide attention of researchers due to their low cost, good stability, and great antimicrobial property (Priya et al. 2020).

NPs have been synthesized conventionally by chemical or physical techniques. However, these methods suffer many disadvantages due to the involvement of expensive operations, toxic chemicals, and large energy consumption (Kocabas et al. 2020). To overcome the above challenges, researchers turn their attention to biological method, which is carried out by microorganisms and plants (Mohamed et al. 2021). However, the microorganisms-mediated synthesis of NPs is a complicated process and often leads to biological contaminants (Mali et al. 2019). Therefore, the synthesis of NPs by plants may be a better choice and also known as "green synthesis" or "eco-friendly synthesis" (Devipriya and Roopan 2017). Green synthesis of NPs is simple and can be produced on a large scale (Rafique et al. 2020). Different plant-derived extracts are abundant, cheap, and easily available. More importantly, plants contain numerous and varied phytochemicals like flavonoids, polyphenols, terpenoids, and alkaloids, which can serve as reducing and capping reagents in the green synthesis process of NPs (Veisi et al. 2021).

Responsible Editor: Gangrong Shi

✉ Yanfang Ren
yanfangren@126.com

[1] School of Environmental and Safety Engineering, Changzhou University, Changzhou, Jiangsu 213164, People's Republic of China

[2] Jiangsu Petrochemical Safety and Environmental Engineering Research Center, Changzhou 213164, People's Republic of China

Some plant extracts have been successfully applied to the green synthesis of NPs, such as *Houttuynia cordata* (Chen et al. 2021), *Ocimum tenuiforum* (Sharma et al. 2020), and *Salvia officinalis* (Okaiyeto et al. 2020). However, it is found that the physical and chemical properties of green synthesized NPs were affected by plant species and synthesis conditions (Kamali et al. 2019; Tshireletso et al. 2021). Khaldari et al. (2021) found that the types and concentrations of plant extracts had great influence on the morphology of synthesized CuO NPs. Kamali et al. (2019) and Kocabas et al. (2020) found that pH obviously affected the particle size of CuO NPs. Kamali et al. (2019) also found that with more rise of the reaction temperature, more precipitation or agglomeration occurred in the synthesis of CuO NPs. In addition, Tshireletso et al. (2021) found that the type of citrus peel affected the particle size and antimicrobial property of CuO NPs. The particle sizes of CuO NPs synthesized from lemon, orange, and tangerine peel extracts were 50, 74, and 70 nm, respectively. CuO NPs synthesized from lemon peel extract has good antibacterial effect, but CuO NPs synthesized from orange peel extract has no antibacterial effect.

Alpinia officinarum Hance is an aromatic rhizome belonging to the *Zingiberaceae* family and mainly distributed in the south of China. *A. officinarum* has anti-inflammatory, anticancer, analgesia, and diuretic properties as well as antioxidant effects and has been widely used as traditional medicine and dietary food (Qu et al. 2021). The main components of *A. officinarum* have been isolated and are flavonoids, diphenyl heptanes, volatile oils, glycosides, etc. (Hoang et al. 2021). It is reported that flavonoids are the most involved substance in the green synthesis process of NPs (Sarkar et al. 2020). Therefore, *A. officinarum* may be a promising source for green synthesis of NPs. However, there is no report of the green synthesis of CuO NPs by using the *A. officinarum* as reducing agent.

Anthracnose caused by *Colletotrichum gloeosporioides* is the most common and harmful fungal disease in mango production, which often leads to 30 ~ 60% postharvest loss (Ren et al. 2020). At present, anthracnose was controlled mainly by organic chemical fungicides, such as prochloraz fungicide (Ntsoane et al. 2019). However, long-term, extensive, and unreasonable use of these chemical agents leads to the development of fungal-resistant strains. In addition, the residues of chemical fungicides can also be toxic to humans and environment (Pei et al. 2020). Thus, it is urgent to explore safe, efficient, and environmental-friendly alternatives to resolve these problems. Green-synthesized NPs are regarded as a kind of eco-friendly fungicide for controlling plant pathogens (Vanathi et al. 2016). Vanathi et al. (2016) have reported potential antifungal properties of *Eichhornia* synthesized CuO NPs against plant fungal pathogens like *Fusarium culmorum* and *Aspergillus niger*. In addition, Henam et al. (2019) found that CuO NPs synthesized by *Euphorbia helioscopia* exhibited significant antifungal activity against *Cladosporium herbarum* owing to its nano size and oxidative damage. However, the antifungal effects of green synthesized CuO NPs on *C. gloeosporioides* were not studied fully.

Herein, the purpose of this research is to (1) explore the potential of CuO NPs synthesized from *A. officinarum* extract and optimize the synthesis process; (2) investigate the potential antifungal activities and its possible mechanism of *A. officinarum* synthesized CuO NPs against *C. gloeosporioides*. It is expected this work may provide a promising eco-friendly fungicide to control postharvest diseases and prolong the shelf life of mango fruit.

Materials and methods

Plant and chemicals

Dry rhizome powder of *A. officinarum* was purchased from Yulin Shengdingju Primary Chinese Herbal Medicine Co., Ltd., China. The precursor copper sulfate pentahydrate ($CuSO_4 \cdot 5H_2O$) was obtained from Sinopharm Chemical Reagent Co., Ltd, China.

Fungal pathogen

C. gloeosporioides was isolated from infected mango fruit and stored in Environmental Biology Laboratory of Changzhou University.

Preparation of *A. officinarum* extract

Dry rhizome powder of *A. officinarum* (10 g) was mixed with 100 mL deionized water using a stirrer-heater at 80 °C for 45 min. The mixture was cooled to room temperature and then filtered through filter membrane (0.45 μm). The filtrate was kept at 4 °C for further use (Kocabas et al. 2020).

Preparation and optimization of synthesis parameters for CuO NPs

300 mL copper sulfate ($CuSO_4$) solution (40 $mmol \cdot L^{-1}$) and 100 mL *A. officinarum* extract were mixed. The concentration of $CuSO_4$ was based on the results of our preliminary experiment (Supplementary materials, Fig. S1). The pH of the mixture was maintained at 4, which is the initial pH value of the reaction mixture. The mixture was then mixed at 60 °C for 3 h, and the formation of CuO NPs was confirmed by change in color to dark brown. Then, the synthesized CuO NPs were centrifuged at 7000 × g for 10 min. The precipitate was rinsed alternately thrice with deionized water followed by absolute ethanol and then collected and dried

at 60 °C for 10 h. Finally, the precipitate was calcinated at 400 °C for 3 h to remove impurities (Singh et al. 2019).

In order to obtain stable and high-quality CuO NPs, the synthesis conditions were optimized based on the above reaction by changing the parameters including the ratio of *A. officinarum* extract and $CuSO_4$ solution (1:1, 1:2, and 1:3 (v/v)), pH of the reaction mixture (4, 7, and 10) and reaction temperature (30, 60, and 90 °C). In the optimization, only one parameter was varied and the other parameters were kept constant. All the samples were analyzed by UV–visible spectroscopic absorption by reading the adsorption spectrum of CuO NPs between 200 and 800 nm.

Characterization of CuO NPs

The UV–visible spectrum of synthesized CuO NPs was measured by UV–visible spectrophotometer (SHIMADZU UV-2700). X-ray diffraction (X-ray diffractometer, D/MAX2500, $2\theta = 20 \sim 80°$) was employed by to monitor crystallinity and purity of synthesized CuO NPs. The functional groups of CuO NPs and *A. officinarum* extract were investigated by Fourier transform infrared radiation spectroscopy (FT-IR, Nicolet IS50) from 400 to 4000 cm^{-1}. The morphology, particle size, and element composition of CuO NPs were analyzed by a Scanning electron microscope (SEM, Zeiss Sigma 300) configured with the energy dispersive spectroscopy (EDS, Pegasus XM2). Hydrodynamic diameter was determined by dynamic light scattering (DLS) with a Malvern Zetasizer Nano machine. Transmission electron microscopy (TEM, JEM-1400plus) was used to analyze the shape and average size of CuO NPs.

Mycelia growth of *C. gloeosporioides*

Antifungal property of CuO NPs against *C. gloeosporioides* was carried out by mycelial growth following the method of Khan et al. (2020). CuO NPs suspensions were added to 20 mL potato dextrose agar (PDA) medium to achieve final concentrations of $15.625 \sim 8000$ $\mu g \cdot mL^{-1}$. PDA medium without CuO NPs was used as control. In the meantime, PDA medium containing *A. officinarum* extract (10%) served as a positive control. After PDA medium solidification, mycelial plug of 11-day-old fungal pathogens with 6 mm in diameter was deposited in the middle of the PDA medium plates and then incubated at 25 °C. The diameter of mycelia colony was measured after 11 days. The experiment was carried out in triplicates. The inhibitory rate of mycelia growth was calculated according to the following formula:

$$\text{Inhibitory rate}(\%) = \frac{D_1 - D_2}{D_1} \times 100$$

where D_1 is the diameter of mycelia growth in control plate, D_2 is the diameter of mycelia growth in treated plate.

Minimum inhibitory concentration and minimum fungicidal concentration

Spore suspension (1×10^6 spores·mL^{-1}) of *C. gloeosporioides* was prepared according to the method of Ren et al. (2020). A two-fold serial broth dilution method was performed for the determination of minimum inhibitory concentration (MIC) for CuO NPs against *C. gloeosporioides* according to the method of Khan et al. (2020). In this experiment, *C. gloeosporioides* was treated with CuO NPs ($15.625 \sim 8000$ $\mu g \cdot mL^{-1}$) in sterile potato dextrose broth (PDB) medium. Each test tube was then inoculated with 1×10^6 spores·mL^{-1} suspensions and incubated on a rotary shaker at 25 °C for 3 days. The absence of fungal growth was visually checked to define MIC value. The minimum fungicidal concentration (MFC) was determined after MIC treatment by inoculating 100 µL samples on PDA medium plates, where no viable colony was observed on the plate after incubation at 25 °C for 24 h (Li et al. 2021). All experiments were performed in triplicates.

Spore germination rate and germ tube prolongation of *C. gloeosporioides*

The effects of CuO NPs on spore germination and germ tube prolongation of *C. gloeosporioides* were assayed according to Ren et al. (2020). 100 µL of spores of *C. gloeosporioides* (1×10^6 spores·mL^{-1}) were inoculated into 5 mL PDB medium containing CuO NPs at MIC, and the PDB medium without CuO NPs was used as control. The cultures were incubated at 25 °C on a rotary shaker at 150 rpm for 12 h. The spore germination and germ tube prolongation were examined at 3, 6, 9, and 12 h after inoculation. Approximately 200 spores were randomly observed using biomicroscope (NE600). A spore was considered germinated when the length of germ tube was equal to or greater than the diameter of the spore. Germination rate was expressed as the percentage of germinated spores out of the total spores evaluated. Germ tube length was assayed with an ocular micrometer. Each treatment was replicated three times.

Cellular leakage

The soluble protein, soluble sugar, and nucleic acid leakage from mycelia of *C. gloeosporioides* treated with (or without) CuO NPs was examined according to the method of Zhu et al. (2021).

Oxidative stress and membrane lipid peroxidation

The superoxide anion (O_2^-) production rate was determined following the method of Elstner and Heupel (1976). The mycelia treated without (as control) or with CuO NPs at MIC were incubated as described above, and collected at 3, 6, 9, and 12 h, respectively. The hydrogen peroxide (H_2O_2) content was measured following the method of Mondal and Choudhuri (1981). The malondialdehyde (MDA) content was measured according to the thiobarbituric acid (TBA) method (Heath and Packer 1968).

Morphological observation of *C. gloeosporioides*

The mycelia morphology of *C. gloeosporioides* was analyzed using the methods described by Li et al. (2021). In brief, mycelia were treated with CuO NPs at MIC for 6 h, and sterile water treatment was taken as the control. Then the mycelia were washed thoroughly with PBS solution (pH 7) and fixed in 2.5% (v/v) glutaraldehyde for 12 h at 4 °C. The hypha was dehydrated in graded series of ethanol solution (30 ~ 100%). Afterwards, the mycelia morphological changes of the *C. gloeosporioides* were observed by SEM (FEI Quanta FEG 250).

Statistical analysis

All the data were presented as the mean ± standard deviation (SD). One-way analysis of variance followed by the least significant difference (LSD) test was used to compare the means between different treatments using IBM SPSS statistics (v26.0) software. *P* value less than 0.05 was considered significantly different.

Results and discussions

UV–vis spectra analysis

The reduction of Cu^{2+} into CuO NPs could be identified by the color change of $CuSO_4$ solution from blue to brown in the existence of *A. officinarum* extract (Fig. 1), which indicated the formation of CuO NPs (Sarkar et al. 2020). With the extension of reaction time, the color of the mixed solution became darker, indicating that more CuO NPs were formed.

The effect of the ratio of *A. officinarum* extract and $CuSO_4$ solution on CuO NPs green synthesis was investigated at a fixed concentration of $CuSO_4$ (40 mmol·L^{-1}), pH 4, and 60 °C. As shown in Fig. 2a, the surface plasmon resonance (SPR) peak intensity and position of the green synthesized CuO NPs was changed when the ratio of extract to $CuSO_4$ solution changed. The enhanced intensity represented the increased concentration, while the blue shift indicated the decreased size of CuO NPs. Our results are similar to those of Kamali et al. (2019). XRD patterns showed that the crystallinity of CuO NPs synthesized was affected by the ratio of extract to $CuSO_4$ solution (Fig. 2d). The sharper peaks were observed in CuO NPs when the volume ratio of *A. officinarum* extract to $CuSO_4$ solution was 1:2. The results from UV–vis spectrum and XRD pattern revealed that the optimal ratio of extract to $CuSO_4$ solution employed for CuO NPs synthesis was 1:2.

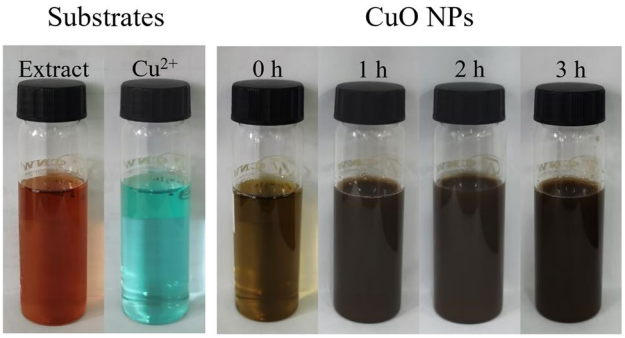

Fig. 1 Color changes of CuO NPs solution at different reaction time

As the pH increased from 4 to 10, the UV–vis absorption peak of CuO NPs also changed (Fig. 2b). Under acidic conditions, all the functional groups possess positive charge and generate repulsive force with positively charged Cu^{2+} due to high proton concentration, which is unfavorable to the formation of CuO NPs. With the increase of pH, the bioavailability of functional groups also increased. This is mainly because polysaccharide molecules and flavonoids with reducibility may change from positive ions to negative ions with the increase of pH value, which will enhance the interaction between them and Cu^{2+} and thus make the reduction reaction easier. Whereas, the CuO NPs became unstable and started to agglomerate at higher pH values such as pH 10. Kamali et al. (2019) also found a similar phenomenon. As shown in Fig. 2e, the crystallinity of the synthesized CuO NPs increased firstly and then drops sharply as the pH value increased. The results showed that pH 7 was the optimal condition for the CuO NPs synthesis using *A. officinarum*.

Figure 2c showed that the SPR peak intensity of the synthesized CuO NPs decreased with the concomitant red shift as the reaction temperature increased from 30 to 90 °C, indicating the reduced concentration and increased size of the synthesized CuO NPs. This result might be due to the destruction of biomolecules capped on the NPs at high temperature, which resulted in agglomeration of CuO NPs and generation of larger particles. The result was agreed with the report by Kamali et al. (2019). The crystallinity of the synthesized CuO NPs changed little at the reaction temperature from 30 to 60 °C; however, it decreased at 90 °C (Fig. 2f).

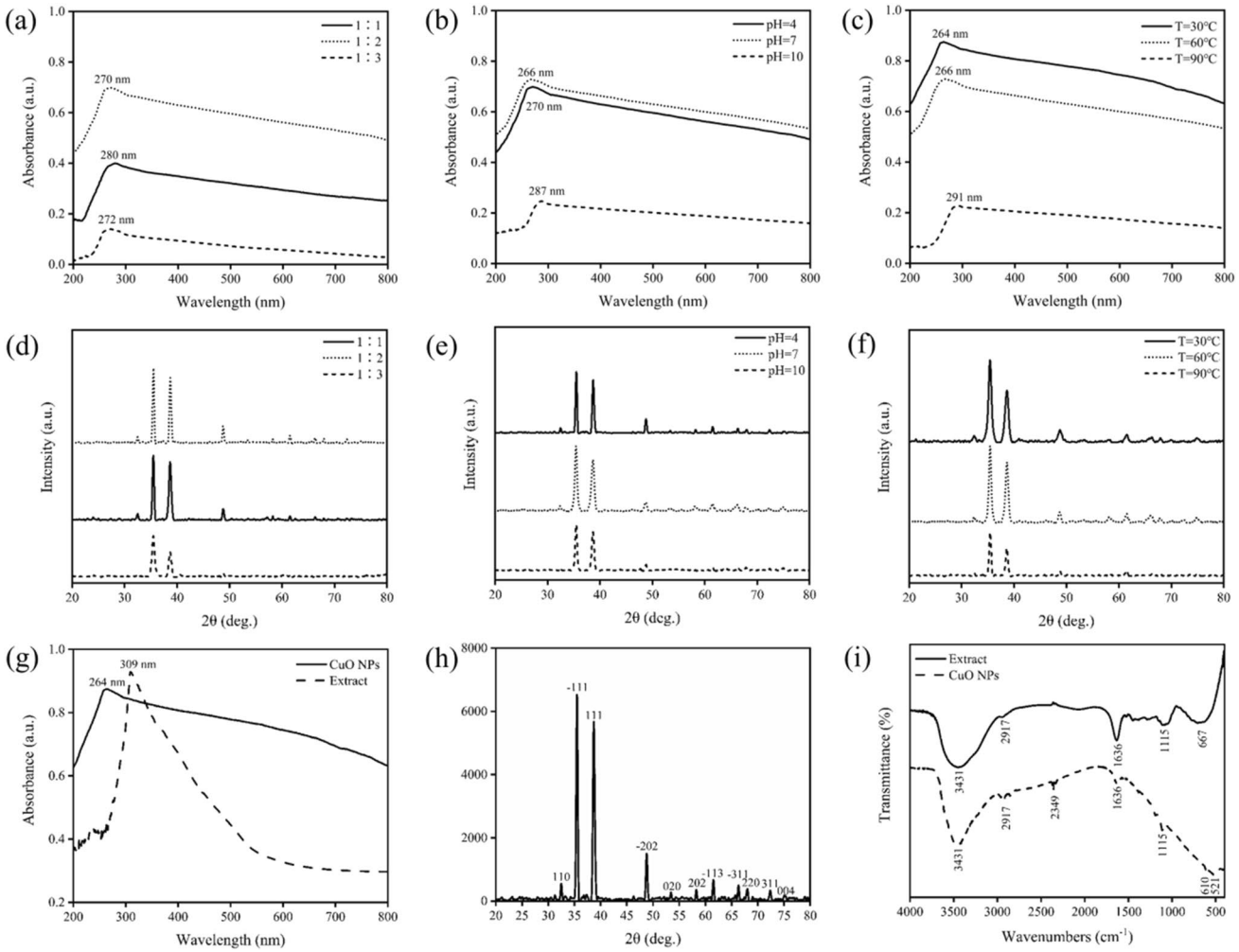

Fig. 2 **a** UV–vis spectra and **d** XRD pattern of the green synthesized CuO NPs under different ratio of *A. officinarum* extract and $CuSO_4$ solution, **b** UV–vis spectra and **e** XRD pattern of the green synthesized CuO NPs with different pH, **c** UV–vis spectra and **f** XRD pattern of the green synthesized CuO NPs with different reaction temperatures, **g** UV–vis spectra of *A. officinarum* extract and green synthesized CuO NPs under optimized conditions, **h** XRD pattern of the green synthesized CuO NPs under optimized conditions, and **i** FT-IR spectra of *A. officinarum* extract and the green synthesized CuO NPs under optimized conditions

Therefore, 30 °C was chosen as the optimum reaction temperature based on the results of UV–vis spectrum and XRD pattern.

To better understand the physical and chemical properties of the synthesized CuO NPs, CuO NPs obtained under the optimized conditions, i.e., the 1:2 ratio of extract and $CuSO_4$ solution, pH 7, and 30 °C, was further characterized using various analytical techniques.

UV–vis analysis

The UV–vis spectra of *A. officinarum* extract and the synthesized CuO NPs under the optimized conditions were shown in Fig. 2g. The CuO NPs exhibited strongest absorbance at 264 nm. The result was similar to the previous study reported by Sankar et al. (2014), who found the UV–vis spectra of CuO NPs synthesized from *Carica papaya* leaves ranged between 250 and 300 nm. However, the peak of *A. officinarum* extract was at 309 nm.

XRD analysis

The observed diffraction sharp peaks position at 32.4°, 35.4°, 38.6°, 48.8°, 53.4°, 58.3°, 61.5°, 66.3°, 67.9°, 72.4°, and 74.9° were assigned to (110), (− 111), (111), (− 202), (020), (202), (− 113), (− 311), (220), (311), and (004), respectively (Fig. 2h). These results were highly consistent with JCPDS Card Number 01–080-1268 of CuO NPs with a monoclinic phase (Naika et al. 2015). No impurity peaks other than CuO were observed in the XRD pattern, indicating the synthesized CuO NPs with high phase purity. The narrow and sharp diffraction peaks indicated that the CuO

NPs were well crystallized in nature. The mean crystallite size (D) was calculated according to the Scherrer equation:

$$D = \frac{K\lambda}{\beta\cos\theta}$$

where K is the dimension constant (0.9), λ is X-ray wavelength (0.15406 nm), β is the value of full width at half maximum, θ is half diffraction angle (Weldegebrieal 2020). The size of the CuO NPs was calculated as 50.56 nm.

FT-IR analysis

FT-IR spectrum clearly displayed a prominent peak around 3431 cm^{-1} (Fig. 2i), indicating the existence of $-OH$ functional group and $-NH_2$ bending. This supported the fact that *A. officinarum* extracts were rich in polyphenols, which could serve as reducing agents (Sarkar et al. 2020). The stretching vibration peak at 2917 cm^{-1} indicated C-H bond stretching and the presence of amine group (Akintelu et al. 2020). The peak at 2349 cm^{-1} was credited to CO_2 vibration in the atmosphere (Rafique et al. 2020). The peak at 1636 cm^{-1} depicted C = O bond stretching, and it may also be the N–H bending vibration and C-N bond vibration (Anand et al. 2020; Kalia et al. 2021). The absorption band at 1115 cm^{-1} linked to C-O bond stretching, which was originated from the biomolecules of the extract. In addition, peaks at 667 cm^{-1} in FT-IR spectrum of *A. officinarum* extract corresponded to aromatic ring and C-H bending vibration, presented in the flavonoids, carotenoids, saponins, and glycosides constituents of the plant extract. The peaks of CuO NPs around 610 cm^{-1} and 521 cm^{-1} belonged to the stretching vibration of Cu–O bond, further corroborating the

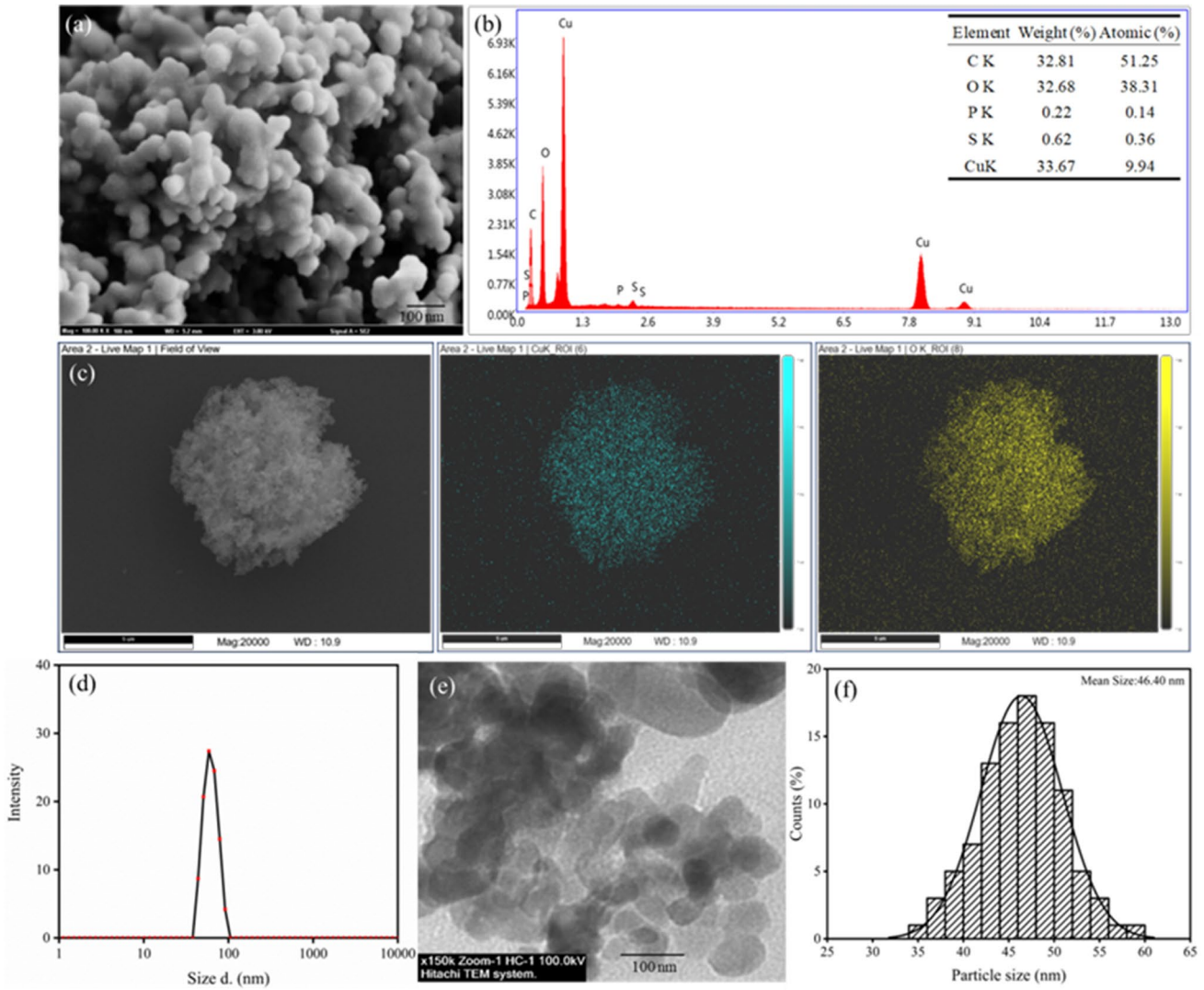

Fig. 3 **a** SEM image, **b** EDS spectra, **c** X-ray atomic mapping, **d** DLS spectra, **e** TEM image, and **f** the particle size dispersion of the CuO NPs

formation of CuO NPs (Weldegebrieal 2020). After calcinations, the FT-IR spectra of CuO NPs displayed the absence or decrease of strong stretching and vibration peaks for some organic compounds of *A. officinarum*. It may be that high-temperature calcinations decompose some plant components on the surface of NPs (Hosseini-Koupaei et al. 2019).

SEM and EDS analysis

SEM image indicated the defined spherical morphology of the prepared CuO NPs (Fig. 3a). The strong signals from the copper and oxygen atoms were observed by EDS (Fig. 3b), confirming the formation of pristine CuO NPs (Nagaraj et al. 2019). The EDS spectrum also showed a strong carbon element peak, and other weak signals such as Ca and S atoms, which was correspond to the phytochemicals from *A. officinarum* extract bonded to CuO NPs. Besides, the X-ray atomic mapping was executed to demonstrate the distribution of constituent elements in the CuO NPs, and it clearly exhibited the uniform distribution of Cu and O atoms over the surface (Fig. 3c).

DLS analysis

Hydrodynamic diameter of CuO NPs measured using DLS was given in Fig. 3d. The average hydrated particle size of CuO NPs is 62.36 nm. It is worth noting that the hydrodynamic diameter is not the physical size of particles, because it contains the sphere of hydration up to the slip plane (Sarkar et al. 2020).

TEM analysis

TEM image illustrated uniformly dispersed spherical CuO NPs particles (Fig. 3e), which was consistent with the SEM image (Fig. 3a). The particle size of CuO NPs were between 35 and 60 nm, and the mean size of CuO NPs measured was 46.40 nm (Fig. 3f), which was smaller than the hydrated particle size (62.36 nm) measured by DLS. The difference might be due to the influence of the biomolecules covering

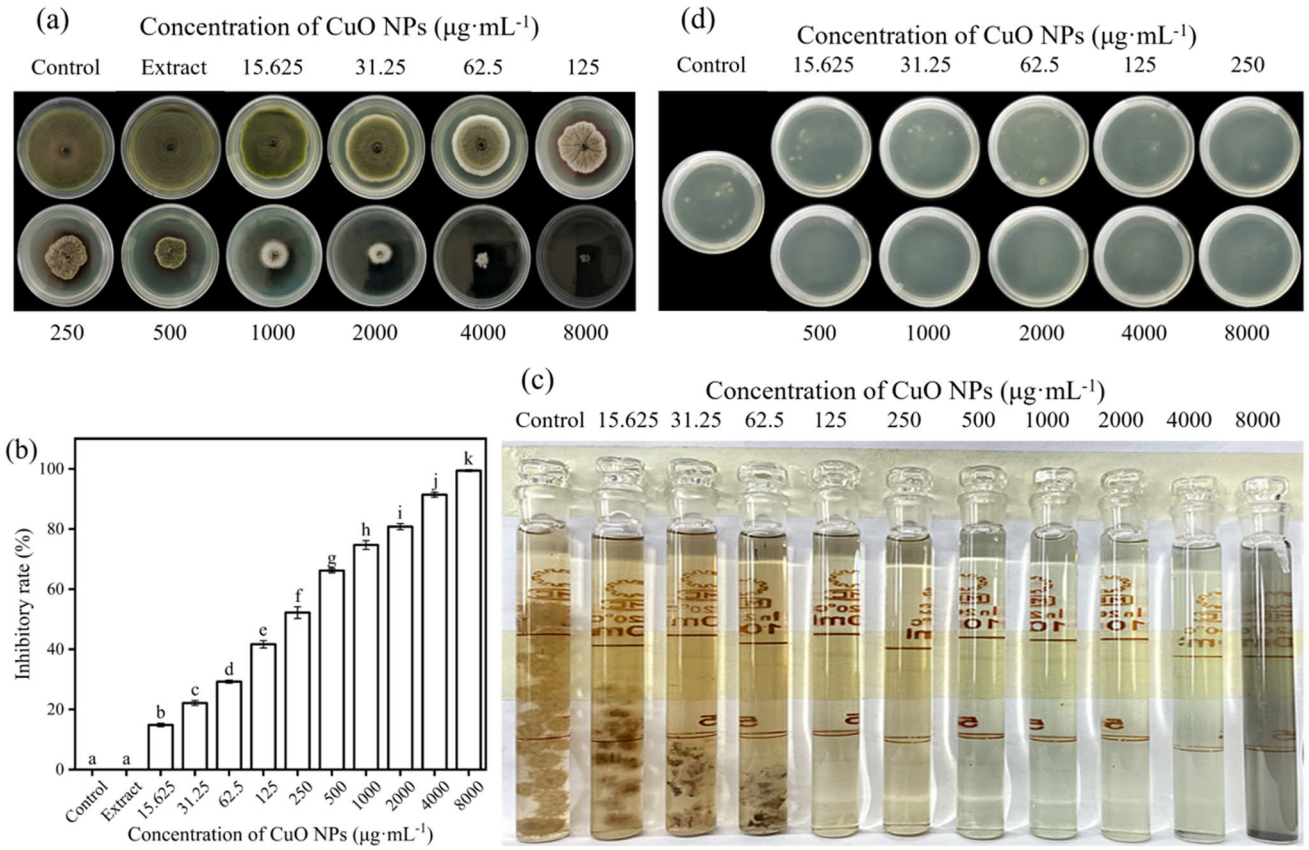

Fig. 4 **a** Photographs of the fungal mycelium growth of *C. gloeosporioides* on PDA plates contained *A. officinarum* extract and 0 ~ 8000 μg·mL^{-1} of CuO NPs after 11 days of incubation, **b** Inhibitory rate of *A. officinarum* extract and 0 ~ 8000 μg·mL^{-1} CuO NPs on mycelium growth of *C. gloeosporioides* after 11 days of incubation, **c** MIC image of CuO NPs against *C. gloeosporioides* in PDB medium, **d** MFC image of CuO NPs against *C. gloeosporioides* on PDA plate. Bars indicate the SD of the means. Values marked with different lowercase letters show an obvious difference between the CuO NPs treatments and the control at $P < 0.05$ based on LSD test

the NPs surface and the Brownian motion (Li et al. 2021). Similar results were also reported in *Coriandrum sativum* synthesized CuO NPs by Sarkar et al. (2020). In addition, the average particle size of *A. officinarum* synthesized CuO NPs was smaller than those synthesized by *Camellia sinensis* and *Lavandula anguistifolia* extract (Khaldari et al. 2021).

Effect of *A. officinarum* synthesized CuO NPs on the fungal growth of *C. gloeosporioides*

As shown in Fig. 4a, CuO NPs significantly inhibited the growth of *C. gloeosporioides* in a dose-dependent manner. This result was agreement with the findings of Vanathi et al. (2016). However, *A. officinarum* extract had no antifungal effect on *C. gloeosporioides*, indicating that the antifungal activity of synthesized NPs comes from CuO NPs (Fig. 4a). Zhang et al. (2020) found that the antimicrobial activity of *A. officinarum* from different organs is different, and it has universal antimicrobial activity against Gram-positive bacteria, but low or no antimicrobial effect against Gram-negative bacteria and fungi. When the concentration of *A. officinarum* synthesized CuO NPs was 1000 μg·mL^{-1}, the inhibition rate of CuO NPs on the growth of *C. gloeosporioides* reached to 74.69% (Fig. 4b). However, Malandrakis et al. (2019) showed that the inhibition rate of CuO NPs at the same concentration on *C. gloeosporioides* growth was about 50%. This observation indicated that the *A. officinarum* synthesized CuO NPs possessed stronger antifungal activity. For the quantitative measurement of antifungal activity of the synthesized CuO NPs, the MIC and MFC were determined. The results showed that the MIC and the MFC values of the CuO NPs were 125 μg·mL^{-1} and 500 μg·mL^{-1}, respectively (Fig. 4c, d).

In order to further explore the inhibitory effect and mechanism of the *A. officinarum* synthesized CuO NPs on the

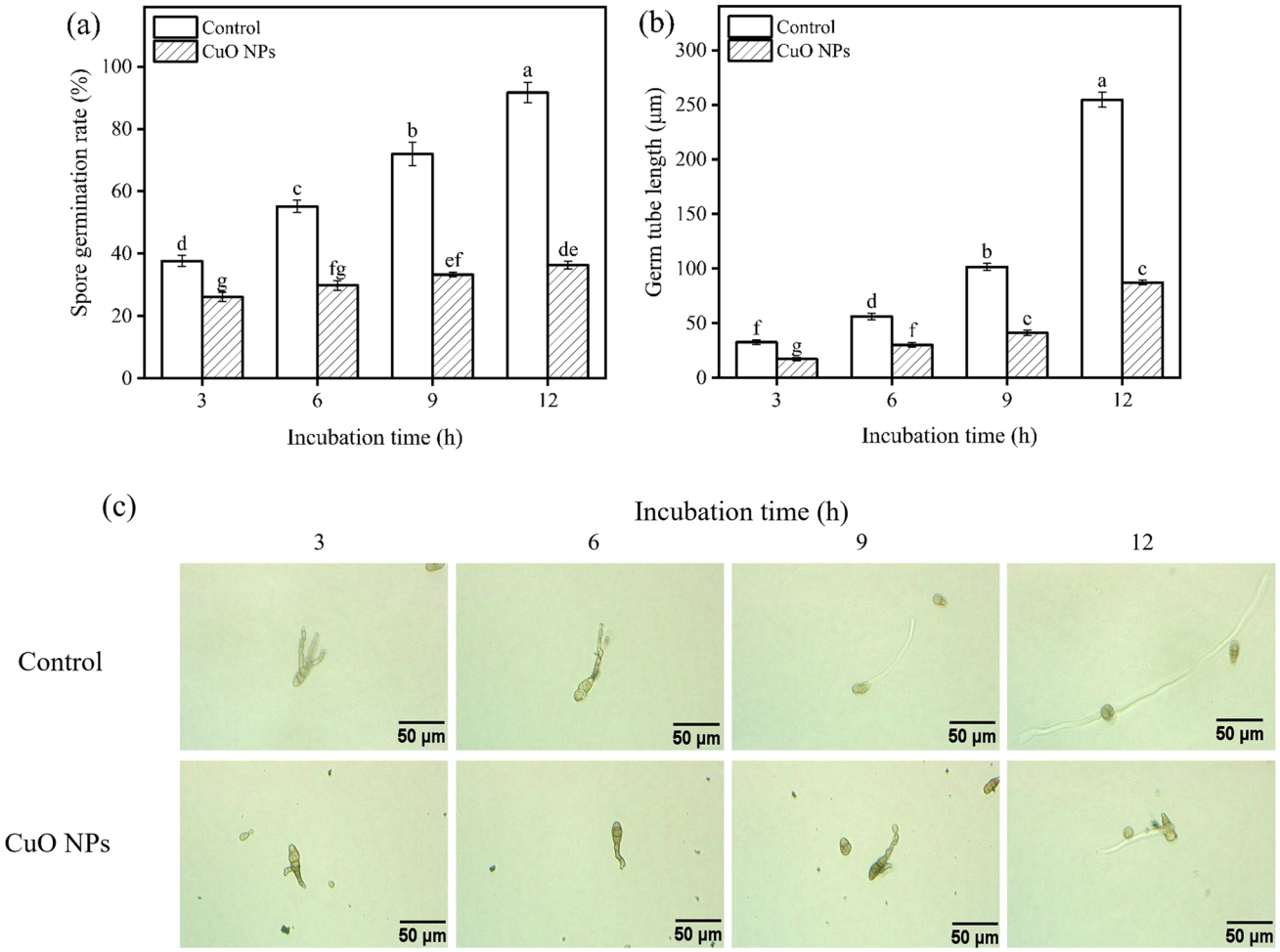

Fig. 5 Inhibitory effects of CuO NPs at MIC on **a** spore germination, **b** germ tube length, and **c** image of the germ tube elongation of *C. gloeosporioides* in vitro. Bars indicate the SD of the means. Values marked with different lowercase letters at different times show an obvious difference between the CuO NPs treatments and the control at $P < 0.05$ based on LSD test

growth of *C. gloeosporioides*, MIC was used as the treatment concentration of CuO NPs for further study.

Effect of *A. officinarum* synthesized CuO NPs on spore germination and germ tube elongation of *C. gloeosporioides*

The spore germination of *C. gloeosporioides* was significantly inhibited by CuO NPs at MIC (Fig. 5a). After incubation for 12 h, the spore germination rate of CuO NPs-treated *C. gloeosporioides* was 39.63% of the control ($P < 0.05$). Similarly, Huang et al. (2021) reported that *Ginkgo biloba* synthesized CuO NPs could significantly inhibit spore germination of *Bipolaris maydis*. Moreover, the germ tube elongation was also significantly inhibited by CuO NPs at MIC, which was only 34.29% of the control after incubation for 12 h ($P < 0.05$) (Fig. 5b, c). This result agrees with the findings of Zhu et al. (2021), who reported that the length of the germ tube of *Alternaria alternate* treated with ZnO NPs was obviously shorter than that in the control group.

Effect of *A. officinarum* synthesized CuO NPs on cellular leakage of *C. gloeosporioides*

The cellular leakage of *C. gloeosporioides* treated with CuO NPs increased with the extension of incubation time (Fig. 6a–c). After 12 h of treatment with CuO NPs, the leakages of soluble protein, soluble sugar and nucleic acid of *C. gloeosporioides* were 3.06, 2.48, and 9.48 times that of the control ($P < 0.05$), respectively. The massive cellular leakage indicated that the integrity of fungal cell membrane was seriously damaged by CuO NPs. However, there was no significant change in the cellular leakage of the control ($P > 0.05$) with the increase of incubation time. Our results were consistent with the results reported by Li et al. (2021), who found that when the cell surface contacted with Ag NPs, the intact cell membrane structure was destroyed, resulting in the leakage of cellular components such as sugar and protein.

Effect of *A. officinarum* synthesized CuO NPs on lipid peroxidation of *C. gloeosporioides*

Excessive reactive oxygen species (ROS) accumulation could result in cell membrane lipid peroxidation and membrane damage. O_2^- and H_2O_2 are two main ROS in organisms (Agnihotri and Seth 2020; Kumar and Seth 2022). MDA is the main product of membrane lipid peroxidation and are often used as an indicator of oxidative damage of the cell membrane (Ren et al. 2017). The results in Fig. 6d–f showed that CuO NPs markedly induced the increase of O_2^-·production rate, H_2O_2, and MDA contents

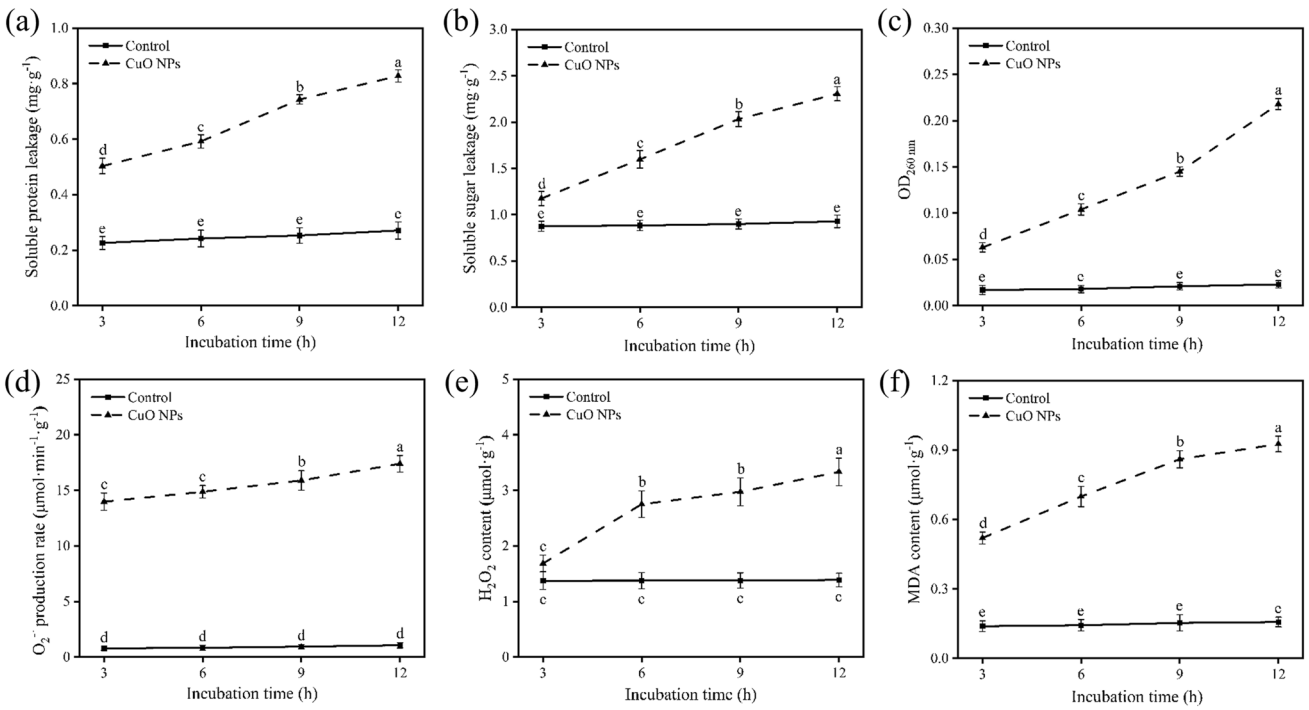

Fig. 6 Effects of CuO NPs at MIC on **a** soluble protein leakage, **b** soluble sugar leakage, **c** nucleic acid leakage, **d** O_2^- production rate, **e** H_2O_2 content, and **f** MDA content of *C. gloeosporioides* in vitro. Bars indicate the SD of the means. Values marked with different lowercase letters at different times show an obvious difference between the CuO NPs treatments and the control at $P < 0.05$ based on LSD test

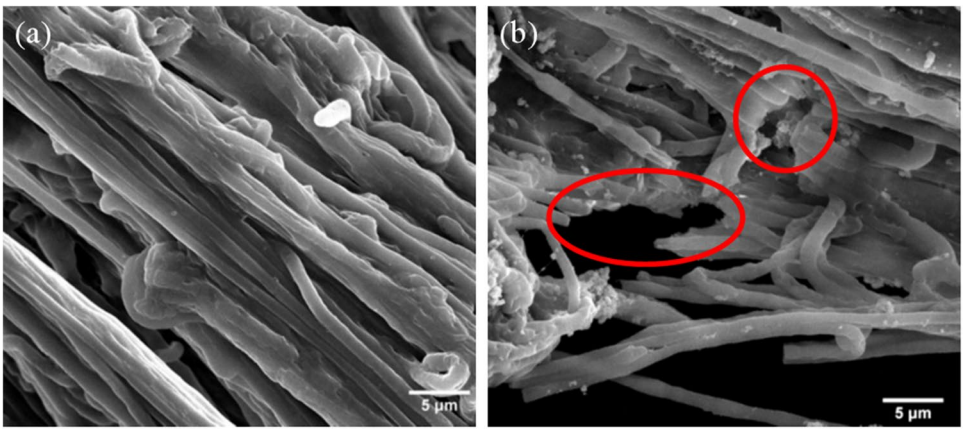

Fig. 7 SEM images of *C. gloeosporioides* mycelia treated with **a** sterile water (as control) and **b** CuO NPs

in *C. gloeosporioides* after 3 h of inoculation ($P < 0.05$). The level of O_2^-, H_2O_2, and MDA in *C. gloeosporioides* subject to CuO NPs treatment at MIC for 12 h were 16.41, 2.40, and 5.90 times of the control. The over production of ROS would aggravate cell damage and the permeability of the membrane was further increased, which led to the massive leakage of cell contents and inhibited the growth of fungal hyphae. Our results agree with the reports by Li et al. (2021), who found that the ROS in the bacteria after Ag NPs treatment was obviously higher than that in the control.

Effect of *A. officinarum* synthesized CuO NPs on fungal morphology of *C. gloeosporioides*

In this study, drastic changes in the external hyphae morphology of *C. gloeosporioides* were observed under treatment with CuO NPs at MIC (Fig. 7b). As shown in Fig. 7a, fungal hyphae treated with sterile water were smooth and free from any damage. However, the hyphae treated with CuO NPs lost their smoothness and broke in many places (Fig. 7b), which would be conducive to the cell leakage. These results indicated that CuO NPs inhibited the growth of *C. gloeosporioides* might be related to malformation of fungal hyphae. Our results resembled the findings of previous work (Pariona et al. 2019). Ahmad et al. (2020) discovered that *A. indica* synthesized CuO NPs clearly damaged hyphae of *D. seriata* and *B. dothidea*, the shape of hyphal walls showed abnormal morphology while mycelia treated with water appeared to remain intact.

Conclusions

CuO NPs were successfully synthesized using $CuSO_4$ and *A. officinarum* extracts. The optimized synthesis parameters of CuO NPs were pH 7, 30 °C, and the ratio of extract and $CuSO_4$ solution at 1:2. The UV–vis spectra of synthesized CuO NPs exhibited characteristic peaks at 264 nm. SEM and TEM images revealed that the particles appeared to be spherical with about 35–60 nm in size. XRD and EDS identified the purity of the synthesized CuO NPs. Moreover, CuO NPs exhibited significant antifungal activity against *C. gloeosporioides*. This might be related to its ability to deform the structure of fungal hyphae, induce excessive ROS accumulation and lipid peroxidation of *C. gloeosporioides*, resulting in the cell membrane injuries and cellular leakage. These results suggested the potential use of green synthesized CuO NPs in challenging fungal phytopathogens.

Supplementary Information The online version contains supplementary material available at https://doi.org/10.1007/s11356-022-24225-9.

Author contribution Chunmei Hu: Conceptualization, Methodology, Writing–original draft, Validation. Wenjia Zhu: Conceptualization, Methodology, Validation. Ying Lu: Methodology, Validation. Yanfang Ren: Project administration, Supervision, Writing—review and editing. Jinyu Gu: Writing—review and editing, Validation. Yaping Song: Writing—editing, Validation. Junyu He: Project administration, Supervision, Writing—review and editing.

Funding This work was funded by the National Natural Science Foundation of China (31660477 and 31360413), the Postgraduate Research & Practice Innovation Program of Jiangsu Province (SJCX21_1187 and KYCX21_2871), and the College Students Innovation and Entrepreneurship Training Program of Changzhou University (2021-A-39).

Data availability The datasets used and/or analyzed during the current study are available from the corresponding author on reasonable request.

Declarations

Ethics approval Not applicable.

Consent for participate Not applicable.

Consent for publication Not applicable.

Competing interests The authors declare no competing interests.

References

Agnihotri A, Seth CS (2020) Does jasmonic acid regulate photosynthesis, clastogenecity, and phytochelatins in *Brassica juncea* L. in response to Pb-subcellular distribution? Chemosphere 243:1–18. https://doi.org/10.1016/j.chemosphere.2019.125361

Ahmad H, Venugopal K, Bhat AH, Kavitha K, Ramanan A, Rajagopal K, Srinivasan R, Manikandan E (2020) Enhanced biosynthesis of copper oxide nanoparticles (CuO-NPs) for their antifungal activity toxicity against major phyto-pathogens of apple orchards. Pharm Res 37:1–12. https://doi.org/10.1007/s11095-020-02966-x

Akintelu SA, Folorunso AS, Folorunso FA, Oyebamiji AK (2020) Green synthesis of copper oxide nanoparticles for biomedical application and environmental remediation. Heliyou 6:e04508. https://doi.org/10.1016/j.heliyon.2020.e04508

Anand MAV, Saravanakumar K, Anbazhagan S, Venkatachalam K, Wang MH (2020) Folic acid functionalized starch encapsulated green synthesized copper oxide nanoparticles for targeted drug delivery in breast cancer therapy. Int J Biol Macromol 164:2073–2084. https://doi.org/10.1016/j.ijbiomac.2020.08.036

Chen HM, Feng XJ, Gao L, Mickymaray S, Paramasivam A, Alfaiz FA, Almasmoum HA, Ghaith MM, Almaimani RA, Ibrahim IAA (2021) Inhibiting the PI3K/AKT/mTOR signalling pathway with copper oxide nanoparticles from *Houttuynia cordata* plant: attenuating the proliferation of cervical cancer cells. Artif Cell Nanomed B 49:240–249. https://doi.org/10.1080/21691401.2021.1890101

Devipriya D, Roopan SM (2017) *Cissus quadrangularis* mediated eco-friendly synthesis of copper oxide nanoparticles and its antifungal studies against *Aspergillus niger*, *Aspergillus flavus*. Mat Sci Eng C-Mater 80:38–44. https://doi.org/10.1016/j.msec.2017.05.130

Elstner EF, Heupel A (1976) Inhibition of nitrite formation from hydroxylammonium-chloride: a simple assay for superoxide dismutase. Anal Biochem 70(2):616–620. https://doi.org/10.1016/0003-2697(76)90488-7

Heath RL, Packer L (1968) Photoperoxidation in isolated chloroplasts: I. Kinetics and stoichiometry of fatty acid peroxidation. Arch Biochem Biophys 125(1):189–198. https://doi.org/10.1016/0003-9861(68)90654-1

Henam SD, Ahmad F, Shah MA, Parveen S, Wani AH (2019) Microwave synthesis of nanoparticles and their antifungal activities. Spectrochim Aata A 213:337–341. https://doi.org/10.1016/j.saa.2019.01.071

Hoang NN, Kodama T, Win NN, Prema P, Do KM, Abe I, Morita H (2021) A new monoterpene from the rhizomes of *Alpinia galanga* and its anti-vpr activity. Chem Biodivers 18:e2100401. https://doi.org/10.1002/cbdv.202100401

Hosseini-Koupaei M, Shareghi B, Saboury AA, Davar F, Sirotkine VA, Hosseini-Koupaei MH, Enteshari Z (2019) Catalytic activity, structure and stability of proteinase K in the presence of biosynthesized CuO nanoparticles. Int J Biol Macromol 122:732–744. https://doi.org/10.1016/j.ijbiomac.2018.11.001

Huang WD, Fang H, Zhang SY, Yu HB (2021) Optimised green synthesis of copper oxide nanoparticles and their antifungal activity. Micro Nano Lett 16:374–380. https://doi.org/10.1049/mna2.12060

Kalia A, Kaur M, Shami A, Jawandha SK, Alghuthaymi MA, Thakur A, Abd-Elsalam KA (2021) Nettle-leaf extract derived ZnO/CuO nanoparticle-biopolymer-based antioxidant and antimicrobial nanocomposite packaging films and their impact on extending the post-harvest shelf life of guava fruit. Biomolecules 11:224–247. https://doi.org/10.3390/biom11020224

Kamali M, Samari F, Sedaghati F (2019) Low-temperature phyto-synthesis of copper oxide nanosheets: its catalytic effect and application for colorimetric sensing. Mat Sci Eng C-Mater 103:109744. https://doi.org/10.1016/j.msec.2019.109744

Khaldari I, Naghavi MR, Motamedi E (2021) Synthesis of green and pure copper oxide nanoparticles using two plant resources *via* solid-state route and their phytotoxicity assessment. RSC Adv 11:3346–3353. https://doi.org/10.1039/d0ra09924d

Khan S, Singh S, Gaikwad S, Nawani N, Junnarkar M, Pawar SV (2020) Optimization of process parameters for the synthesis of silver nanoparticles from *Piper betle* leaf aqueous extract, and evaluation of their antiphytofungal activity. Environ Sci Pollut R 27:27221–27233. https://doi.org/10.1007/s11356-019-05239-2

Kocabas BB, Attar A, Peksel A, Yapaoz MA (2020) Phytosynthesis of CuONPs via *Laurus nobilis*: determination of antioxidant content, antibacterial activity and dye decolorization potential. Biotechnol Appl Bioc 68:889–895. https://doi.org/10.1002/bab.2010

Kumar D, Seth CS (2022) Photosynthesis, lipid peroxidation, and antioxidative responses of *Helianthus annuus* L. against chromium (VI) accumulation. Int J Phytoremediat 24(6):1–10. https://doi.org/10.1080/15226514.2021.1958747

Li W, Qu F, Chen YB, Sun YF, Zhang JJ, Xie GY, You QX, Xu HY (2021) Antimicrobial activity of sliver nanoparticles synthesized by the leaf extract of *Cinnamomum camphora*. Biochem Eng J 172:108050. https://doi.org/10.1016/j.bej.2021.108050

Malandrakis AA, Kavroulakis N, Chrysikopoulos CV (2019) Use of copper, silver and zinc nanoparticles against foliar and soil-borne plant pathogens. Sci Total Environ 670:292–299. https://doi.org/10.1016/j.scitotenv.2019.03.210

Mali SC, Raj S, Trivedi R (2019) Biosynthesis of copper oxide nanoparticles using *Enicostemma axillare* (*Lam.*) leaf extract. Biochem Biophys Rep 20:100699. https://doi.org/10.1016/j.bbrep.2019.100699

Mohamed AA, Abu-Elghait M, Ahmed NE, Salem SS (2021) Eco-friendly mycogenic synthesis of ZnO and CuO nanoparticles for in vitro antibacterial, antibiofilm, and antifungal applications. Biol Trace Elem Res 199:2788–2799. https://doi.org/10.1007/s12011-020-02369-4

Mondal R, Choudhuri MA (1981) Role of hydrogen peroxide in senescence of excised leaves of rice and maize. Biochem Physiol Pflanzen 176(8):700–709. https://doi.org/10.1016/S0015-3796(81)80055-8

Moon SA, Salunke BK, Saha P, Deshmukh AR, Kim BS (2018) Comparison of dye degradation potential of biosynthesized copper oxide, manganese dioxide, and silver nanoparticles using *Kalopanax pictus* plant extract. Korean J Chem Eng 35:702–708. https://doi.org/10.1007/s11814-017-0318-4

Murugesan G, Nachimuthu L, Mariappan R (2019) Copper oxide nanoparticles synthesized using *Eupatorium odoratum*, *Acanthospermum hispidum* leaf extracts, and its antibacterial effects against pathogens: a comparative study. BioNanoScience 9:545–552. https://doi.org/10.1007/s12668-019-00655-7

Nagaraj E, Karuppannan K, Shanmugam P, Venugopal S (2019) Exploration of bio-synthesized copper oxide nanoparticles using *Pterolobium hexapetalum* leaf extract by photocatalytic activity and biological evaluations. J Clust Sci 30:1157–1168. https://doi.org/10.1007/s10876-019-01579-8

Naika HR, Lingaraju K, Manjunath K, Kumar D, Nagaraju G, Suresh D, Nagabhushana H (2015) Green synthesis of CuO nanoparticles using *Gloriosa superba* L. extract and their antibacterial activity. J Taibah Univ Sci 9:7–12. https://doi.org/10.1016/j.jtusci.2014.04.006

Ntsoane ML, Zude-Sasse M, Mahajan P, Sivakumar D (2019) Quality assesment and postharvest technology of mango: a review of its current status and future perspectives. Sci Hortic 249:77–85. https://doi.org/10.1016/j.scienta.2019.01.033

Okaiyeto K, Hoppe H, Okoh AI (2020) Plant-based synthesis of silver nanoparticles using aqueous leaf extract of *Salvia officinalis*: characterization and its antiplasmodial activity. J Clust Sci 32:101–109. https://doi.org/10.1007/s10876-020-01766-y

Pariona N, Mtz-Enriquez AI, Sanchez-Rangel D, Carrion G, Paraguay-Delgadoe F, Rosas-Saito G (2019) Green-synthesized copper nanoparticles as a potential antifungal against plant pathogens. RSC Adv 9:18835–18843. https://doi.org/10.1039/c9ra03110c

Pei SP, Liu RL, Gao HY, Chen HJ, Wu WJ, Fang XJ, Han YC (2020) Inhibitory effect and possible mechanism of carvacrol against *Colletotrichum fructicola*. Postharvest Biol Tec 163:111126. https://doi.org/10.1016/j.postharvbio.2020.111126

Priya DD, Roopan SM, Singh S, Bansal J, Shanavas S, Khan MR, Al-Dhabi NA, Arasu MV, Duraipandiyan V (2020) Phyto-synthesis of CuO nano-particles and its catalytic application in C-S bond formation. Mater Lett 266:127486. https://doi.org/10.1016/j.matlet.2020.127486

Qu HJ, Lin KW, Li XL, Ou HY, Tan YF, Wang M, Wei N (2021) Chemical constituents and anti-gastric ulcer activity of essential oils of *Alpinia officinarum* (Zingiberaceae), *Cyperus rotundus* (Cyperaceae), and their herbal pair. Chem Biodivers 18:e2100214. https://doi.org/10.1002/cbdv.202100214

Rafique M, Shafiq F, Gillani SSA, Shakil M, Tahir MB, Sadaf I (2020) Eco-friendly green and biosynthesis of copper oxide nanoparticles using *Citrofortunella microcarpa* leaves extract for efficient photocatalytic degradation of Rhodamin B dye form textile wastewater. Optik 208:164053. https://doi.org/10.1016/j.ijleo.2019.164053

Ren YF, He JY, Liu HY, Liu GQ, Ren XL (2017) Nitric oxide alleviates deterioration and preserves antioxidant properties in 'Tainong' mango fruit during ripening. Hortic Environ Biote 58:27–37. https://doi.org/10.1007/s13580-017-0001-z

Ren YF, Xue YH, Tian D, Zhang LM, Xiao GY, He JY (2020) Improvement of postharvest anthracnose resistance in mango fruit by nitric oxide and the possible mechanisms involved. J Agr Food Chem 68:15460–15467. https://doi.org/10.1021/acs.jafc.0c04270

Sankar R, Manikandan P, Malarvizhi V, Fathima T, Shivashangari KS, Ravikumar V (2014) Green synthesis of colloidal copper oxide nanoparticles using *Carica papaya* and its application in photocatalytic dye degradation. Spectrochim Aata A 121:746–750. https://doi.org/10.1016/j.saa.2013.12.020

Sarkar N, Sharma RS, Kaushik M (2020) Innovative application of facile single pot green synthesized CuO and CuO@APTES nanoparticles in nanopriming of *Vigna radiata* seeds. Environ Sci Pollut R 28:1–8. https://doi.org/10.1007/s11356-020-11493-6

Sharma S, Kumar K, Thakur N, Chauhan MS (2020) *Ocimum tenuiflorum* leaf extract as a green mediator for the synthesis of ZnO nanocapsules inactivating bacterial pathogens. Chem Pap 74:3431–3444. https://doi.org/10.1007/s11696-020-01177-3

Singh J, Kumar S, Alok A, Upadhyay SK, Rwawt M, Tsang DCW, Bolan N, Kim KH (2019) The potential of green synthesized zinc oxide nanoparticles as nutrient source for plant growth. J Clean Prod 214:1061–1070. https://doi.org/10.1016/j.jclepro.2019.01.018

Tshireletso P, Ateba CN, Fayemi OE (2021) Spectroscopic and antibacterial properties of CuONPs from orange, lemon and tangerine peel extracts: potential for combating bacterial resistance. Molecules 26:586–603. https://doi.org/10.3390/molecules26030586

Vanathi P, Rajiv P, Sivaraj R (2016) Synthesis and characterization of *Eichhornia*-mediated copper oxide nanoparticles and assessing their antifungal activity against plant pathogens. Bull Mater Sci 39:1165–1170. https://doi.org/10.1007/s12034-016-1276-x

Veisi H, Karmakar B, Hemmati Tamoradi T, S, Hekmati M, Hamelian M, (2021) Biosynthesis of CuO nanoparticles using aqueous extract of herbal tea (*Stachys Lavandulifolia*) flowers and evaluation of its catalytic activity. Sci Rep 11:1983–1995. https://doi.org/10.1038/s41598-021-81320-6

Weldegebrieal GK (2020) Photocatalytic and antibacterial activityof CuO nanoparticles biosynthesized using *Verbascum thapsus* leaves extract. Optik 204:164230. https://doi.org/10.1016/j.ijleo.2020.164230

Zhang L, Pan C, Ou Z, Liang X, Shi Y, Chi L, Zhang Z, Zheng X, Li C, Xiang H (2020) Chemical profiling and bioactivity of essential oils from *Alpinia officinarum* Hance from ten localities in China. Ind Crop Prod 153:112583. https://doi.org/10.1016/j.indcrop.2020.112583

Zhu W, Hu C, Ren Y, Lu Y, Song Y, Ji Y, Han C, He J (2021) Green synthesis of zinc oxide nanoparticles using *Cinnamomum camphora* (L.) Presl leaf extracts and its antifungal activity. J Environ Chem Eng 9(6):106659. https://doi.org/10.1016/j.jece.2021.106659